Electronic Supplementary Information (ESI)

Anion recognition in water by a simple bis-squaramide with charge-enhanced acidity

Chen Dong, Kehao Zhang, Junhong Li, Jihao Wang, Wenrui Lyu, Xuanxuan Chen and Xin Wu

Table of Contents

S1. General

All reagents were purchased from commercial sources and used as received. NMR spectra were recorded on Bruker Avance 500 and 600 MHz NMR spectrometers. High resolution mass spectrometry (HRMS) was taken on an iMScope QT.

S2. Syntheses

Step 1 Synthesis of neutral bis-squaramide 2

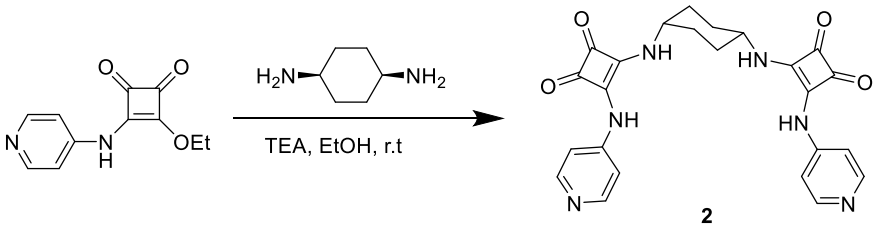

3-ethoxy-4-(pyridin-4-ylamino)-cyclobut-3-ene-1,2-dione was synthesized following a reported procedure.[1] A solution of *cis*-1,4-diaminocyclohexane (0.05 g, 0.5 mmol) and triethylamine (0.06 mL, 3 mmol) in ethanol (15 mL) was added dropwise to a solution of 3-ethoxy-4-(pyridin-4-ylamino)-cyclobut-3-ene-1,2-dione (0.3 g, 1.5 mmol) in ethanol (5 mL). The reaction mixture was stirred at room temperature overnight. A precipitate formed, which was collected by filtration, washed with ethanol (3 × 30 mL), and dried *in vacuo* to afford a pale-yellow solid (0.202 g, 95%). Due to the low solubility of this compound, TBA_2SO_4 was used to solubilize this compound in DMSO-d_6 for NMR characterization.

^{1}H NMR (600 MHz, DMSO-d_6) δ 11.72 (s, 2H), 9.79 (s, 2H), 8.32 (d, J = 5.6 Hz, 4H), 7.75 (s, 4H), 4.19 (d, J = 8.0 Hz, 2H), 2.00 – 1.64 (m, 8H).

^{13}C NMR (150 MHz, DMSO-d_6) δ 184.97, 180.15, 169.92, 164.56, 150.11, 146.97, 112.96, 49.09, 27.90.

HRMS (ESI) *m/z*: $[M+H]^+$ calculated 459.1775, found 459.1772.

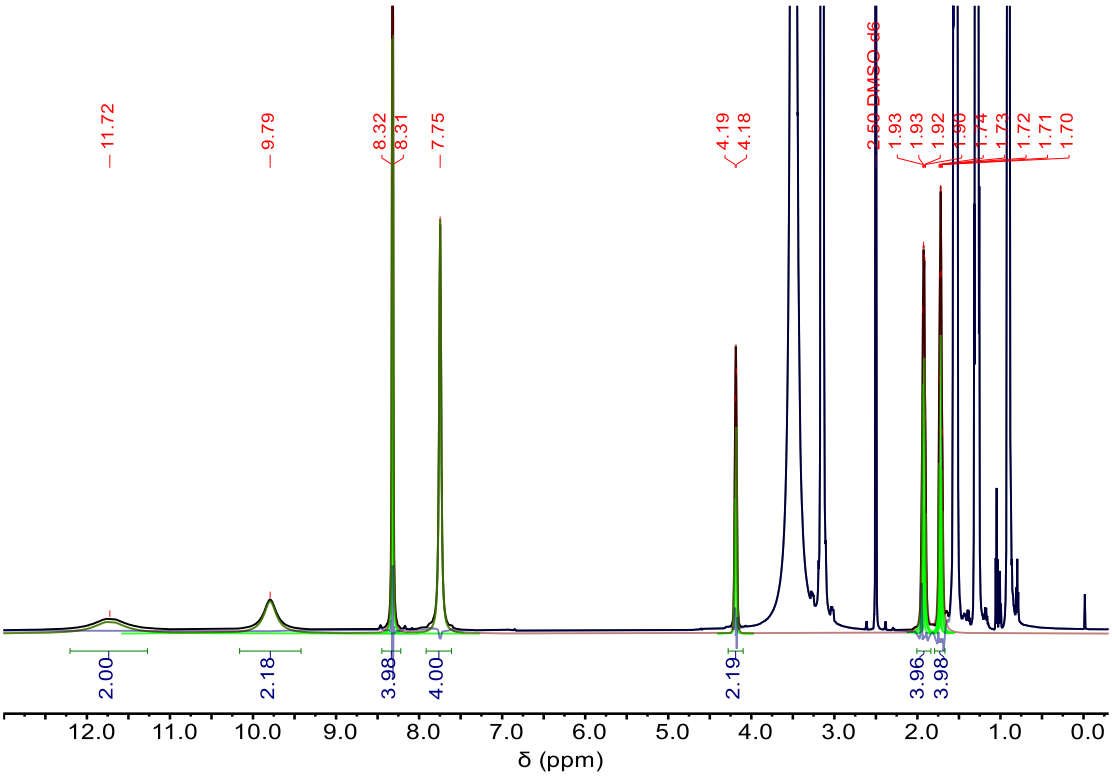

Fig. S1 ^{1}H NMR (600 MHz) of compound **2** in the presence of TBA_2SO_4 in DMSO-d_6.

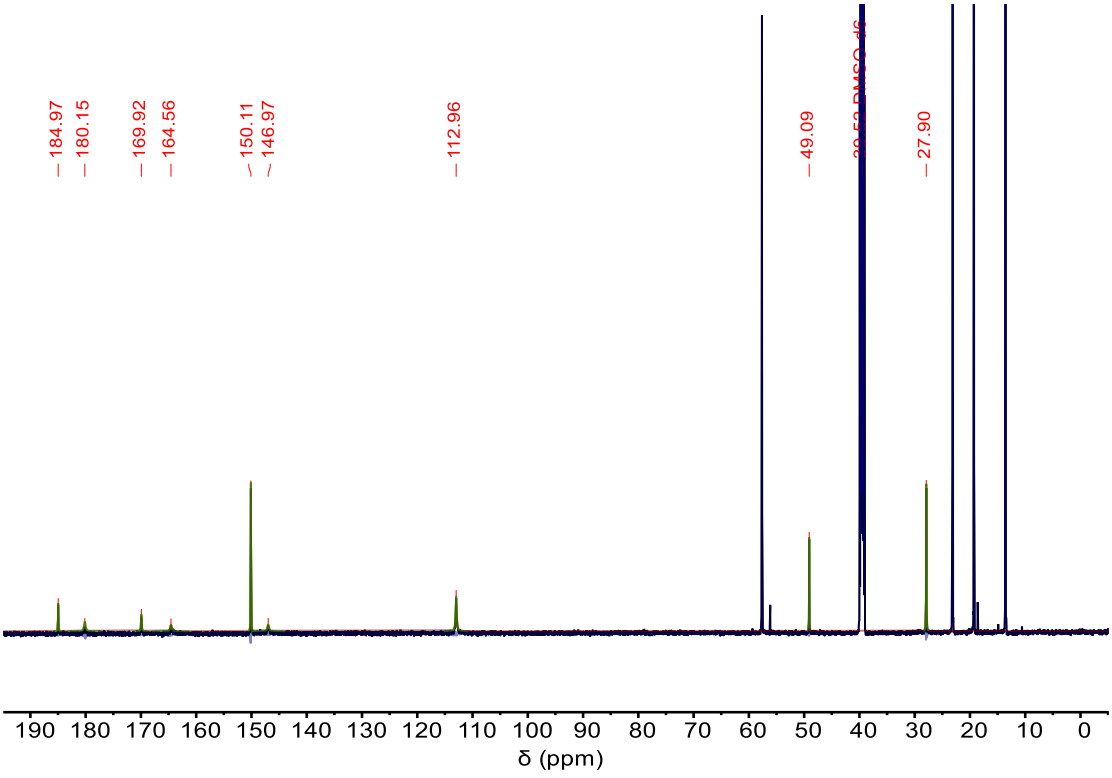

Fig. S2 ^{13}C NMR (150 MHz) of **2** the presence of TBA_2SO_4 in DMSO-d_6.

Step 2 Synthesis of $1^{2+}\cdot 2I^-$

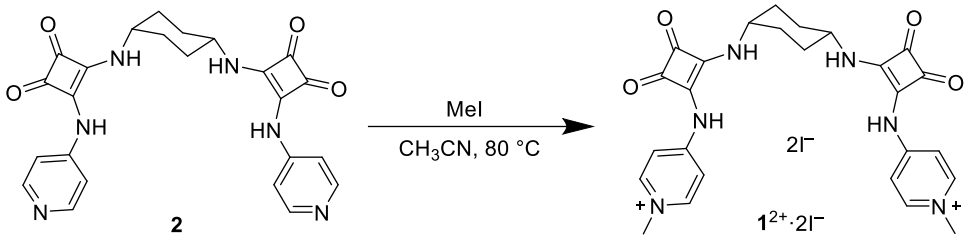

Methyl iodide (0.6 g, 4 mmol) was added dropwise to a suspension of compound **2** (0.05 g, 0.11 mmol) in acetonitrile (5 mL). The reaction mixture was stirred at 80 °C overnight, then cooled to room temperature and concentrated *in vacuo* to give a precipitate. Acetonitrile (10 mL) was added, and the solvent was evaporated again. The residue was dissolved in DMF, and precipitation was induced by addition of DCM. The solid was collected and dried *in vacuo* to afford a pale-yellow powder (0.053 g, 49%). The less-than-quantitative yield is due to incomplete methylation of **2**.

^{1}H NMR (600 MHz, D_2O) δ 8.41 (d, J = 6.9 Hz, 2H), 7.81 (d, J = 6.6 Hz, 2H), 4.25 (s, 2H), 4.15 (s, 6H), 2.05 – 1.79 (m, 8H).

^{13}C NMR (150 MHz, DMSO-d_6) δ 186.47, 180.05, 170.84, 160.24, 151.07, 145.54, 113.58, 50.57, 45.82, 28.42.

MALDI-TOF MS *m/z*: $[M–H]^-$ calculated 741.01887, found 741.01854.

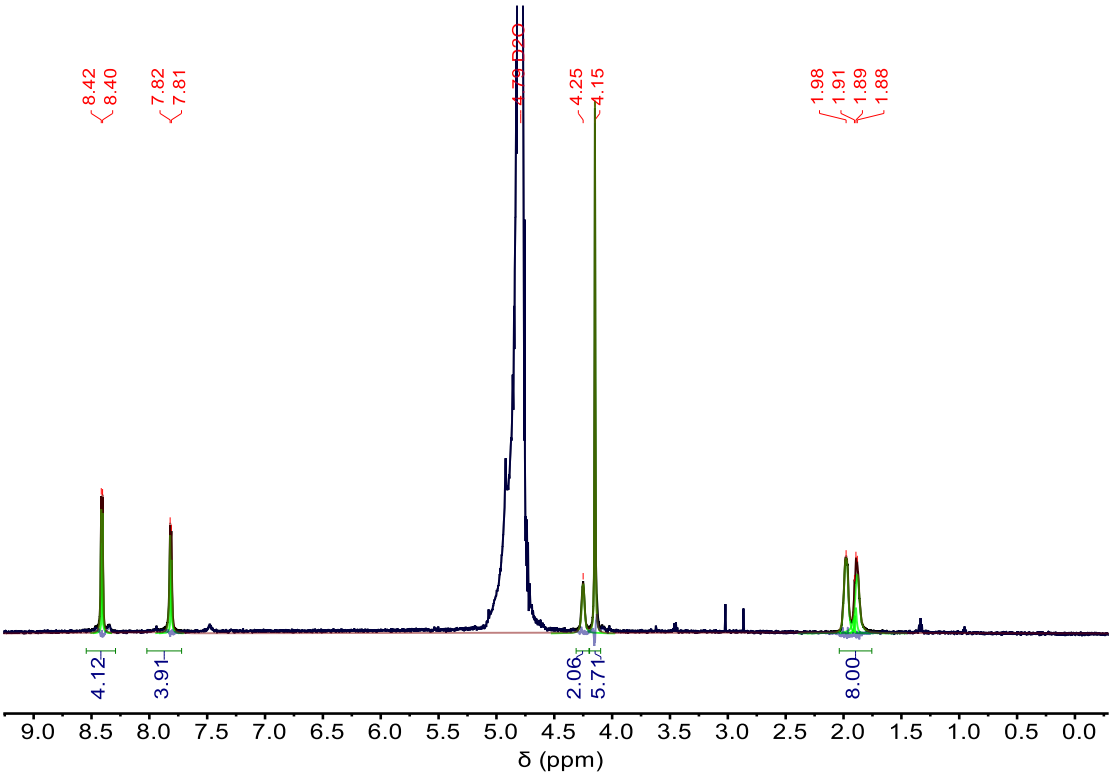

Fig. S3 ^{1}H NMR (600 MHz) of $\mathbf{1}^{2+}\cdot 2I^-$ in D_2O. The minor unidentified resonances are impurities, which are present at <5% relative to $\mathbf{1}^{2+}$.

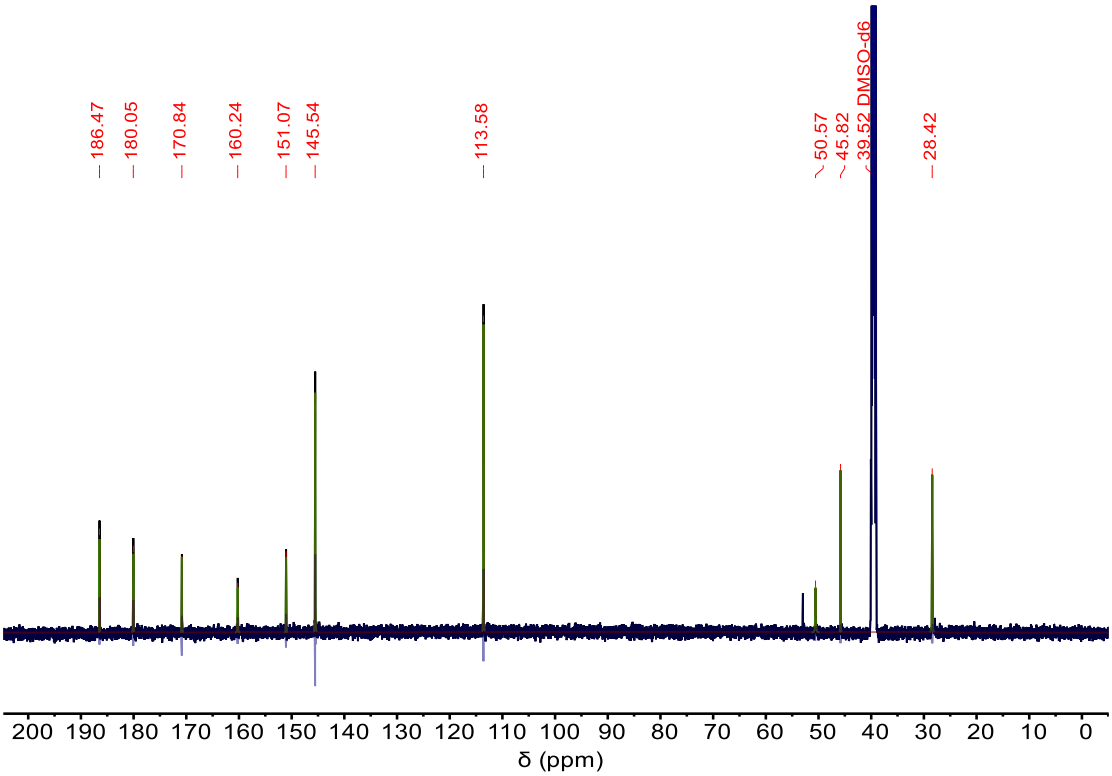

Fig. S4 ^{13}C NMR (150 MHz) of $\mathbf{1}^{2+}\cdot 2I^{-}$ in D_2O.

S3. pK_a determination

The pK_a of receptor $\mathbf{1}^{2+}\cdot 2I^-$ was determined by potentiometric titration. An aqueous solution of $\mathbf{1}^{2+}\cdot 2I^-$ (2.0 mM, 5 mL) was titrated with NaOH (0.20 M), and the pH change was monitored in real time with a pH meter. No ionic strength buffer was used. The ionic strength of the solution was in the range of 6–4.5 mM before precipitate formation. Precipitation of the receptor occurred with 0.75 equiv. of NaOH, with a concomitant drop of the solution pH. The data before precipitation were fitted to a diprotic acid model using BSTAC version 0.1.1., giving pK_{a1} = 6.71 ± 0.01 and pK_{a2} = 7.95 ± 0.06 (mean ± SD) from two independent measurements. Because pK_{a2} is outside the range of fitted data and likely inaccurate, only pK_{a1} is reported in the main article.

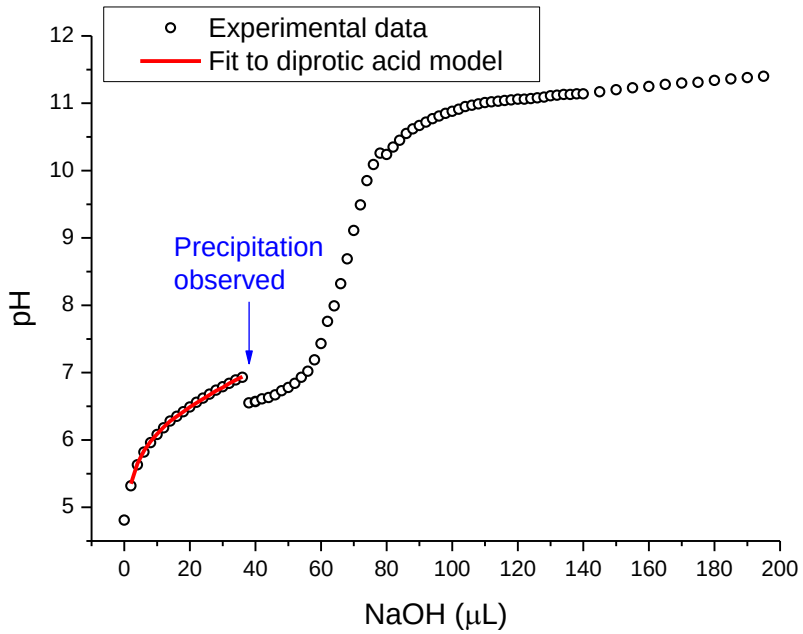

Fig. S5 Potentiometric titration of $\mathbf{1}^{2+}\cdot 2I^-$ (2 mM) by NaOH in H_2O at 298 K. The receptor precipitates at 0.75 equiv. of NaOH, leading to a drop of solution pH. The data before precipitation were fitted to a diprotic acid model to give pK_{a1} = 6.71 ± 0.01 and pK_{a2} = 7.95 ± 0.06 (mean ± SD) from two independent measurements.

S4. ^{1}H NMR titrations

Increasing concentrations of a salt was titrated to a solution of $\mathbf{1}^{2+}\cdot 2I^-$ in 9:1 H_2O/D_2O. ^{1}H NMR spectra were acquired using the zgesgppe pulse sequence to suppress the water signal. The chemical shifts of CH signal(s) with varying salt concentrations were fitted to a 1:1 or 2:1 binding model using BindFit (supramolecular.org), OriginPro or Musketeer[2] software.

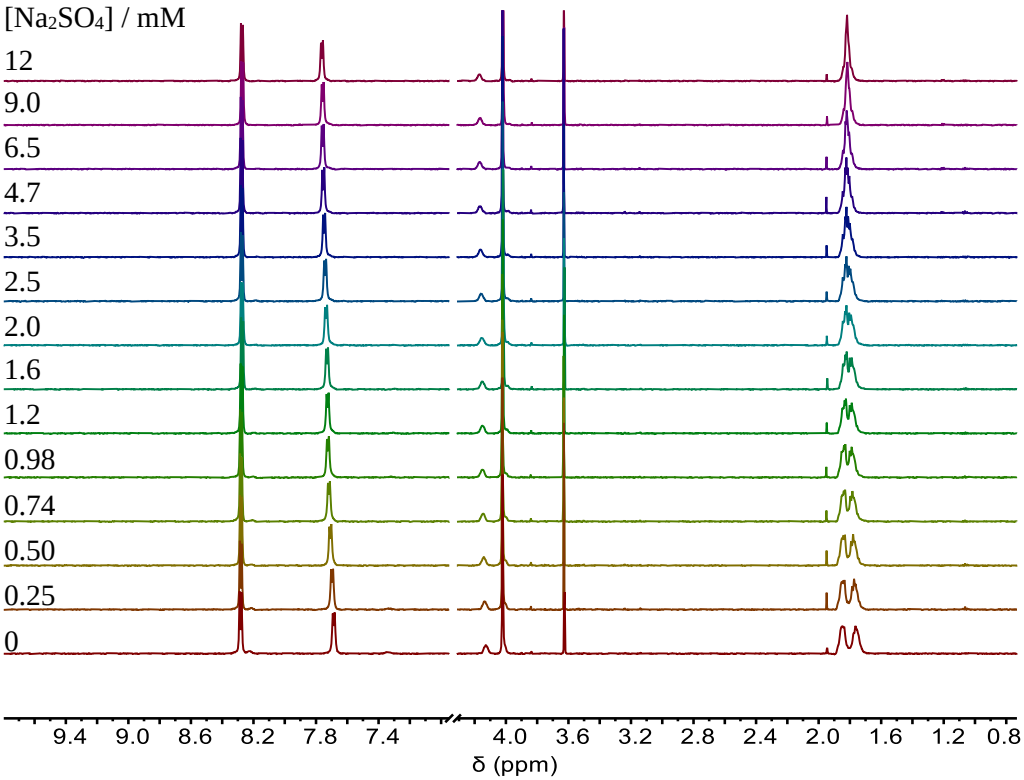

Fig. S6 ^{1}H NMR (600 MHz) titration of $\mathbf{1}^{2+}\cdot 2I^-$ (1 mM) with Na_2SO_4 in 9:1 H_2O/D_2O at 298 K. The coalescence of cyclohexane CH_2 signals at 1.8 ppm might be due to acceleration of the interconversion between two equivalent chair conformations of the cyclohexyl ring, or the stabilisation of the two-fold symmetric twist-boat conformation, induced by SO_4^{2-} binding.

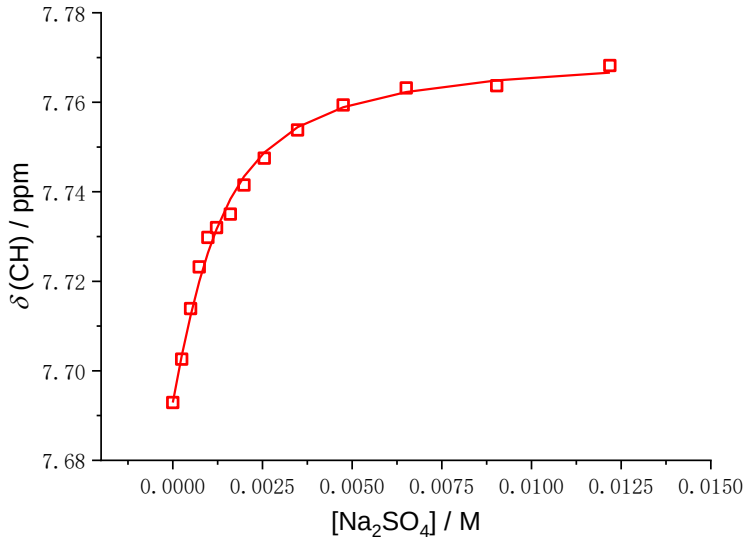

Fig. S7 Fitting of the aryl CH to a 1:1 binding model. *K* values of 1320 and 1520 M^{-1} were determined from two independent titrations, giving mean ± SD as 1420 ± 140 M^{-1}.

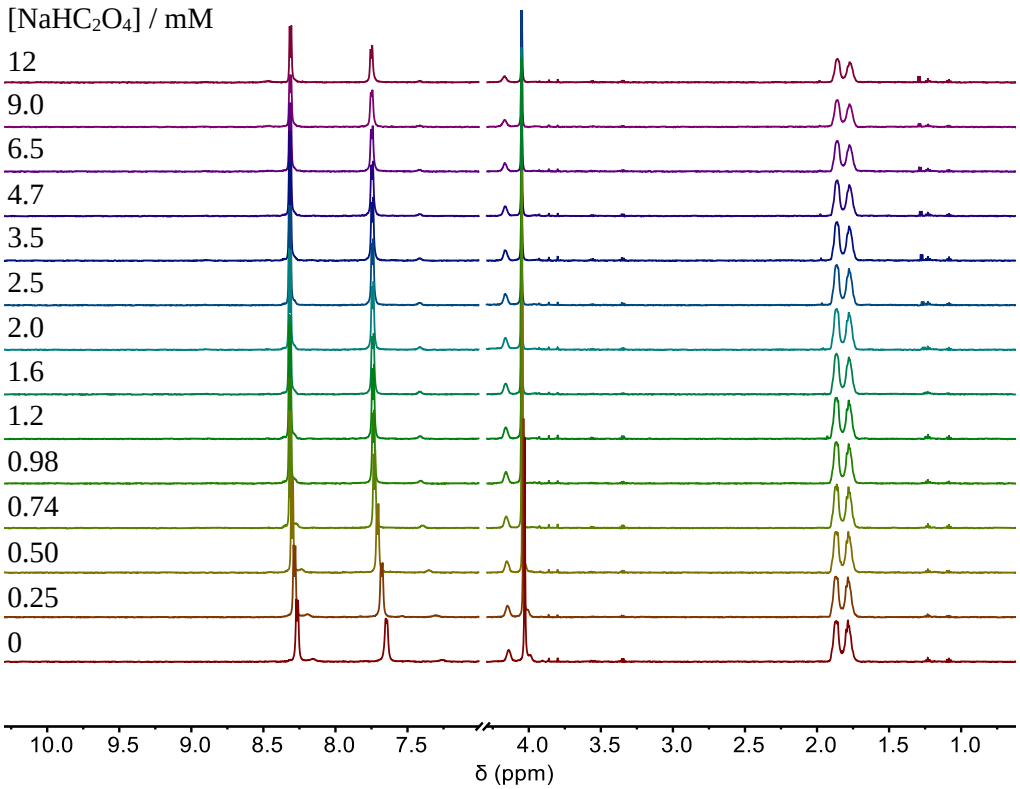

Fig. S8 ^{1}H NMR (600 MHz) titration of $\mathbf{1}^{2+}\cdot 2I^{-}$ (1 mM) with $NaHC_2O_4$ in 9:1 H_2O/D_2O at 298 K.

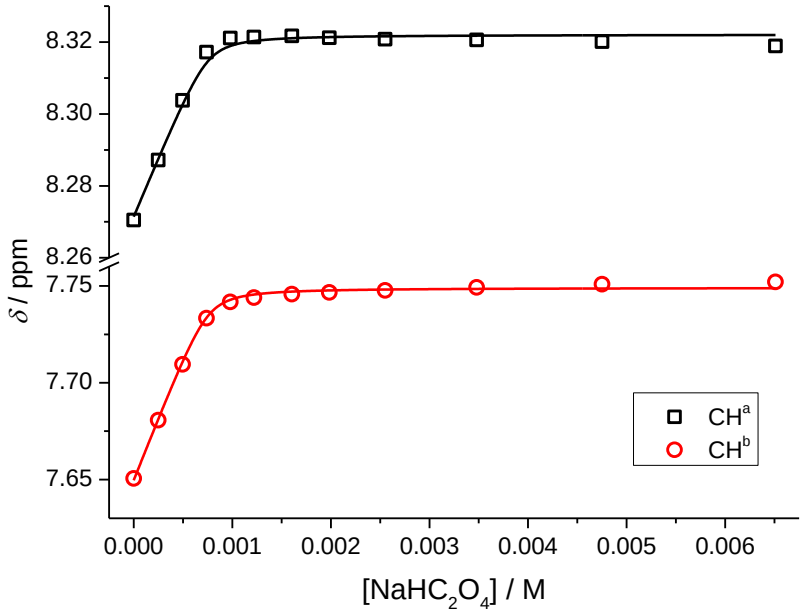

Fig. S9 Global fitting of two aryl CH signals to a 1:1 binding model. *K* values of 5.5×10^4 and 4.4×10^4 M^{-1} were determined from two independent titrations, giving mean ± SD as $(5.0 \pm 0.8) \times 10^4$ M^{-1}. Precipitation was observed with > 6 mM of $NaHC_2O_4$, and therefore higher concentration data was not used for fitting.

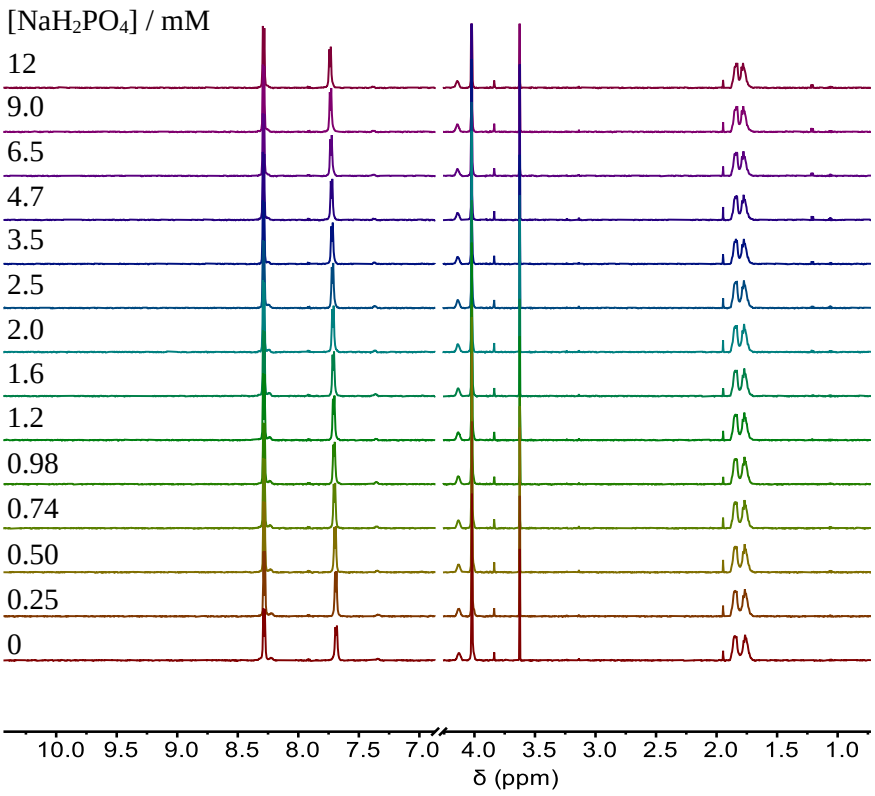

Fig. S10 ^{1}H NMR (600 MHz) titration of $\mathbf{1}^{2+}\cdot 2I^{-}$ (1 mM) with NaH_2PO_4 in 9:1 H_2O/D_2O at 298 K.

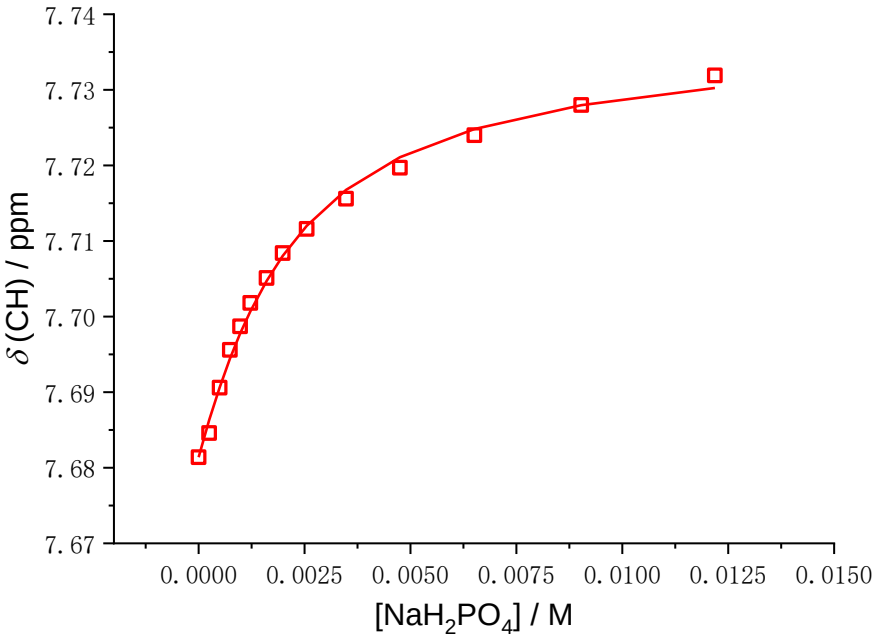

Fig. S11 Fitting of aryl CH^{b} to a 1:1 binding model. *K* values of 590 and 660 M^{-1} were determined from two independent titrations, giving mean ± SD as 630 ± 50 M^{-1}.

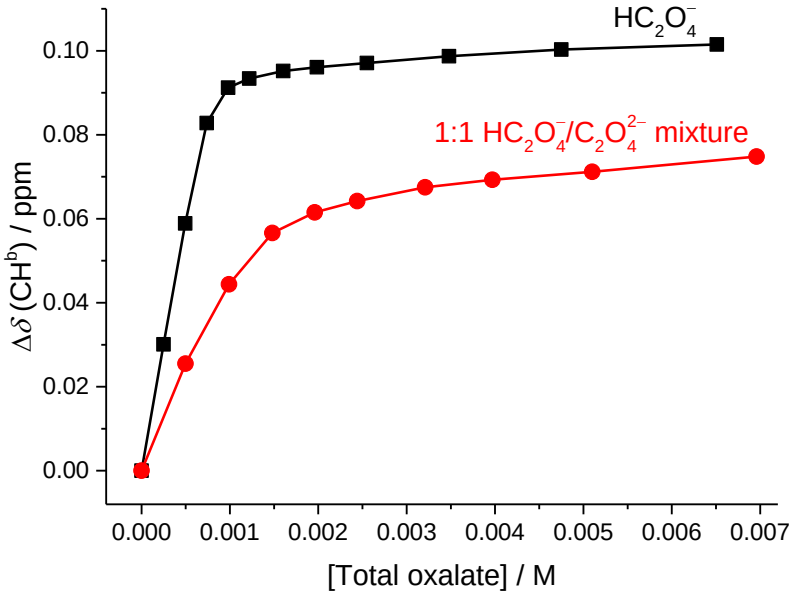

Fig. S12 Comparison of CH^b changes induced by $HC_2O_4^-$ and a 1:1 mixture of $HC_2O_4^-/C_2O_4^{2-}$ in 9:1 H_2O/D_2O at 298 K. $HC_2O_4^-$ induced more pronounced chemical shift changes than a mixture of $HC_2O_4^-/C_2O_4^{2-}$, confirming that the NMR responses observed in the $HC_2O_4^-$ titration experiment (Figs. S8-S9) are induced by $HC_2O_4^-$ rather than the $C_2O_4^{2-}$ in equilibrium with $HC_2O_4^-$.

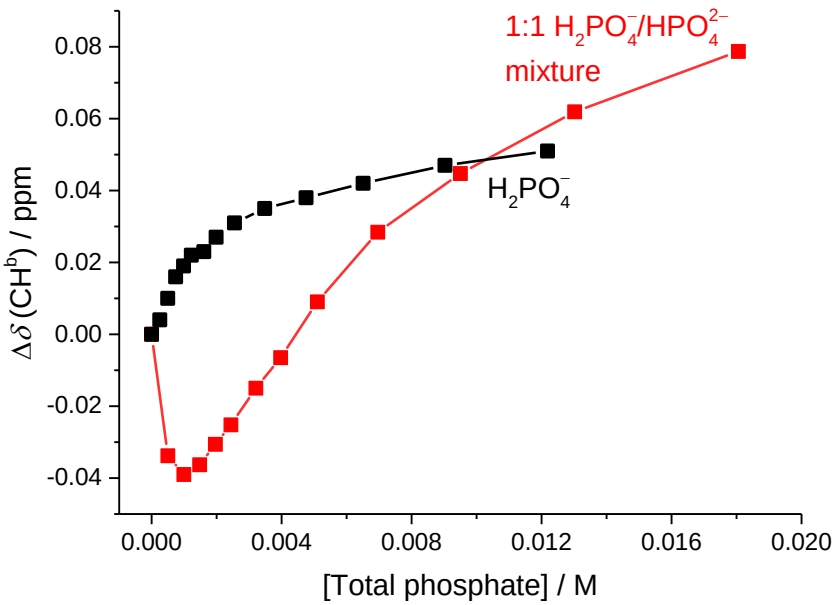

Fig. S13 Comparison of CH^b changes induced by NaH_2PO_4 and a 1:1 mixture of NaH_2PO_4/Na_2HPO_4 in 9:1 H_2O/D_2O at 298 K. For the titration with $H_2PO_4^-/HPO_4^{2-}$ (pH ~ 7.2), CH^b underwent initial upfield shift due to partial deprotonation of $\mathbf{1}^{2+}$ (pK_a = 6.71). Further increasing the phosphate concentration led to dominance of anion binding over deprotonation, shifting the CH^b downfield. The chemical shift change induced by a mixture of $H_2PO_4^-/HPO_4^{2-}$ at high concentrations is greater than the saturated change induced by $H_2PO_4^-$. These results confirm that the responses observed in the $H_2PO_4^-$ titration experiment (Figs. S10-S11) are induced by $H_2PO_4^-$ rather than the HPO_4^{2-} in equilibrium with $H_2PO_4^-$ - this is because if HPO_4^{2-} binding were responsible, the $H_2PO_4^-$ titration curve would approach the value observed for $H_2PO_4^-/HPO_4^{2-}$ (ΔCH^b ~0.08 ppm), rather than saturating at ΔCH^b of 0.06.

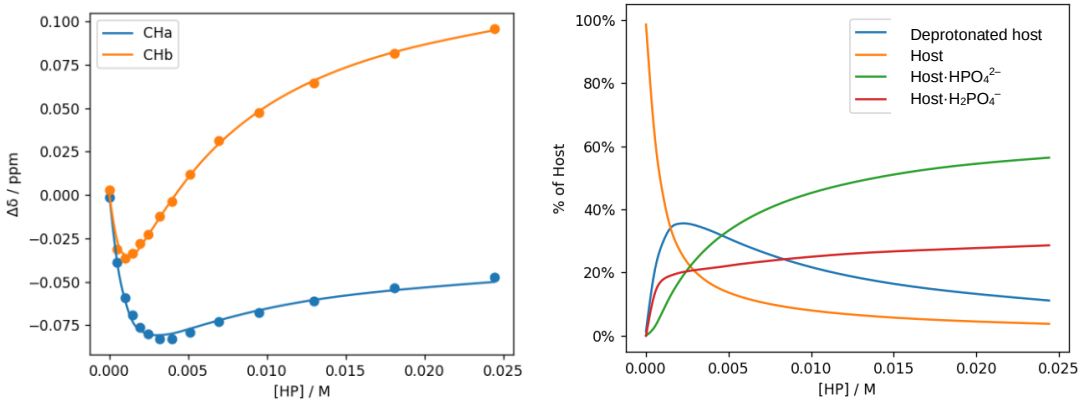

Fig. S14 By performing a multi-equilibria analysis (Musketeer software) of the titration data using 1:1 $H_2PO_4^-/HPO_4^{2-}$ mixture, fixing the known values of pK_a of $\mathbf{1}^{2+}$, pK_a of $H_2PO_4^-$ and binding constant/chemical shift changes of $\mathbf{1}^{2+}/H_2PO_4^-$ complexation, the HPO_4^{2-} binding constant for $\mathbf{1}^{2+}$ can be determined to be 1300 M^{-1}. Saturated ΔCH^b values were calculated to be 0.18 and 0.06 ppm for HPO_4^{2-} and $H_2PO_4^-$, consistent with the higher charge density of HPO_4^{2-} than $H_2PO_4^-$.

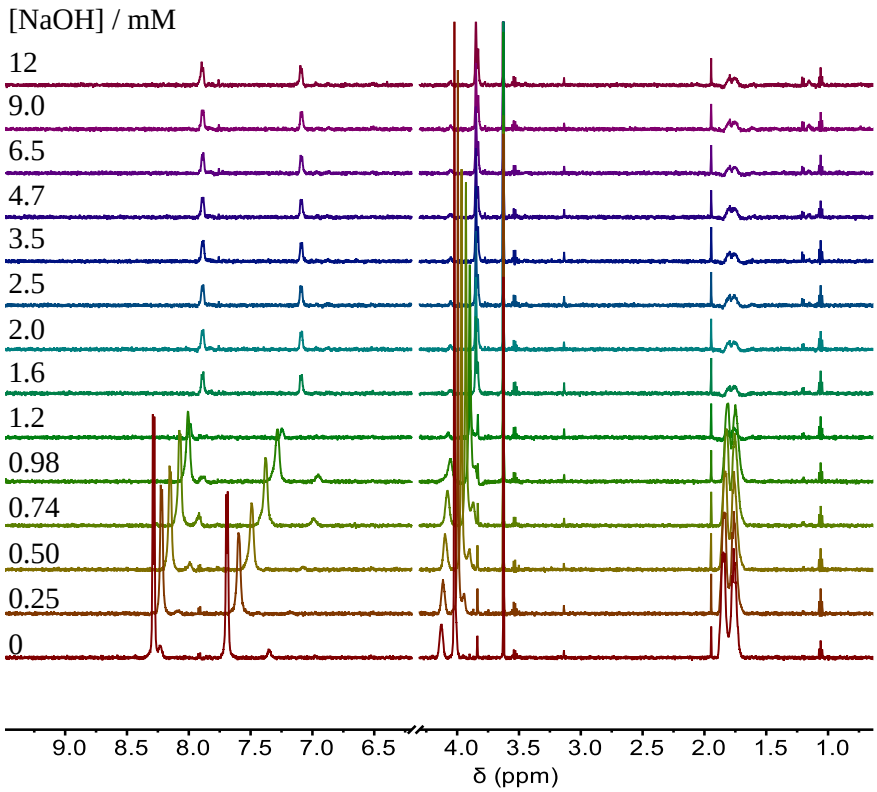

Fig. S15 ^{1}H NMR (600 MHz) titration of $\mathbf{1}^{2+}\cdot 2I^{-}$ (1 mM) with NaOH in 9:1 H_2O/D_2O at 298 K.

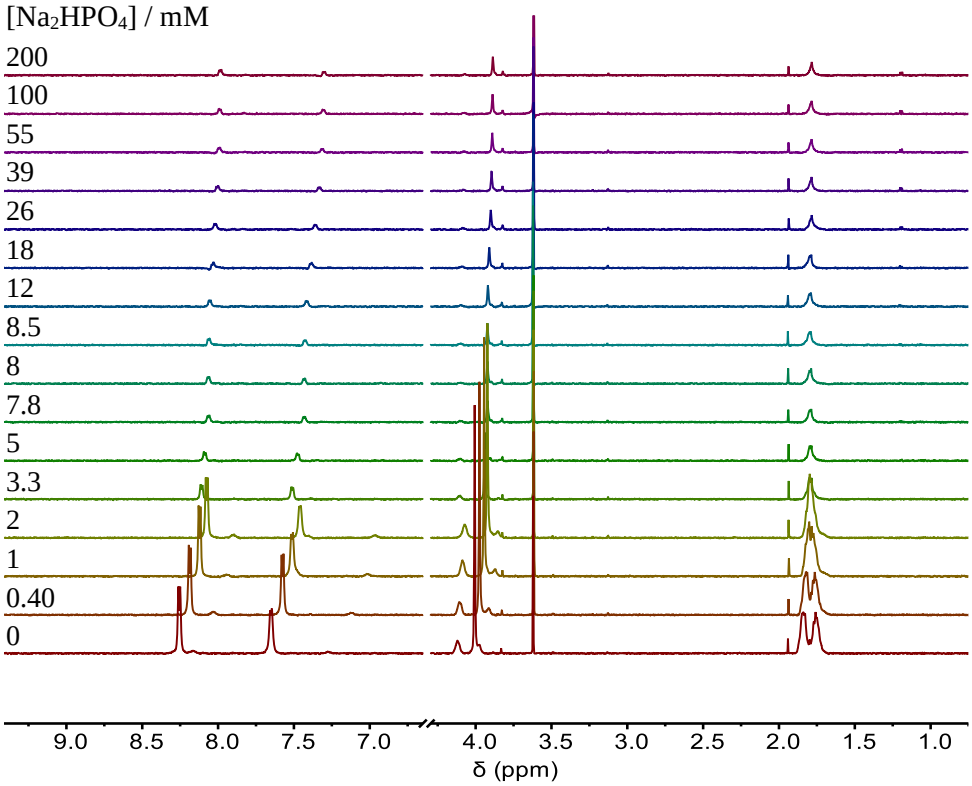

Fig. S16 ^{1}H NMR (600 MHz) titration of $\mathbf{1}^{2+}\cdot 2I^{-}$ (1 mM) with Na_2HPO_4 in 9:1 H_2O/D_2O at 298 K. The chemical shift changes are similar to those observed with NaOH titration, indicating deprotonation of $\mathbf{1}^{2+}$.

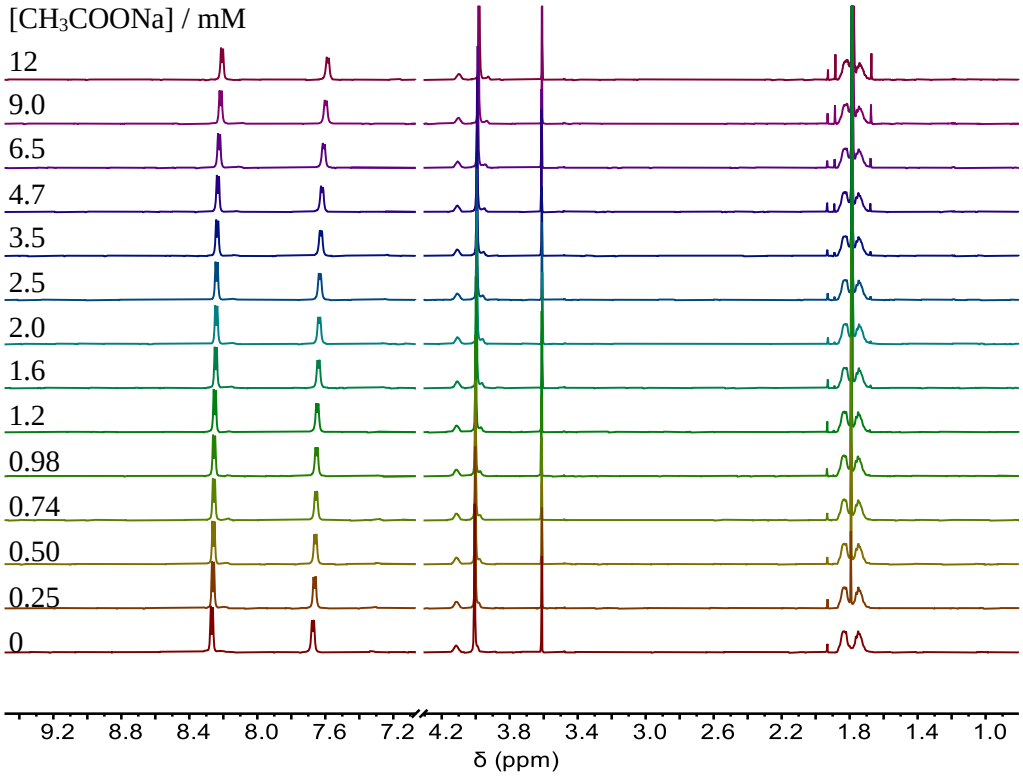

Fig. S17 ^{1}H NMR (600 MHz) titration of $\mathbf{1}^{2+}\cdot 2I^{-}$ (1 mM) with CH_3COONa in 9:1 H_2O/D_2O at 298 K. The trend of chemical shift changes, compared with that observed with NaOH titration, indicates partial deprotonation of $\mathbf{1}^{2+}$.

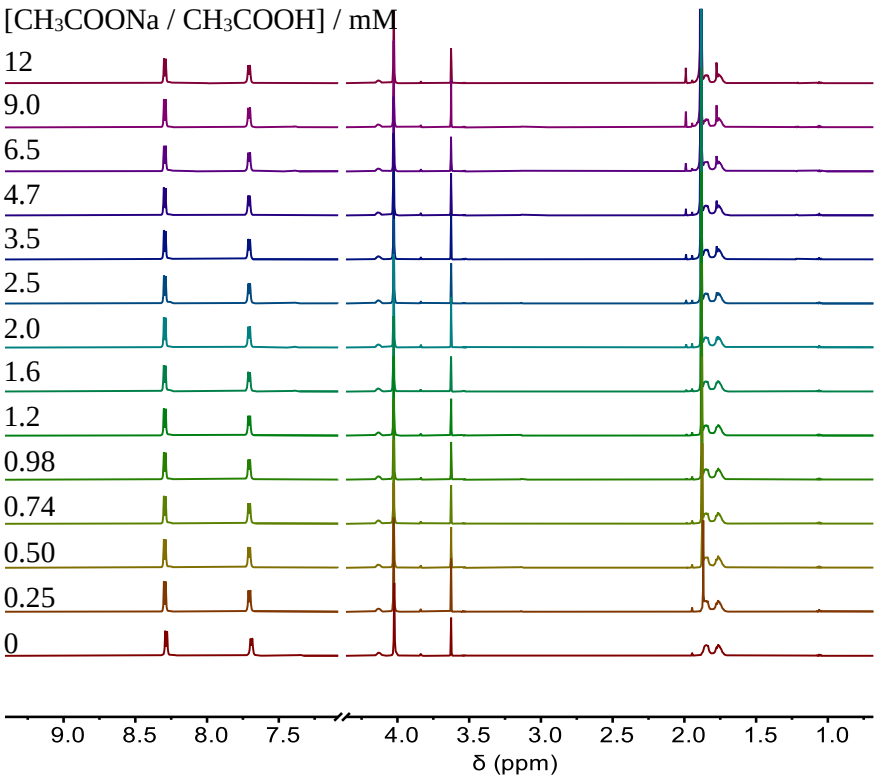

Fig. S18 ^{1}H NMR (600 MHz) titration of $\mathbf{1}^{2+}\cdot 2I^{-}$ (1 mM) with a 1:1 mixture of CH_3COONa/CH_3COOH in 9:1 H_2O/D_2O at 298 K. No chemical shift changes are observed, indicating no acetate binding.

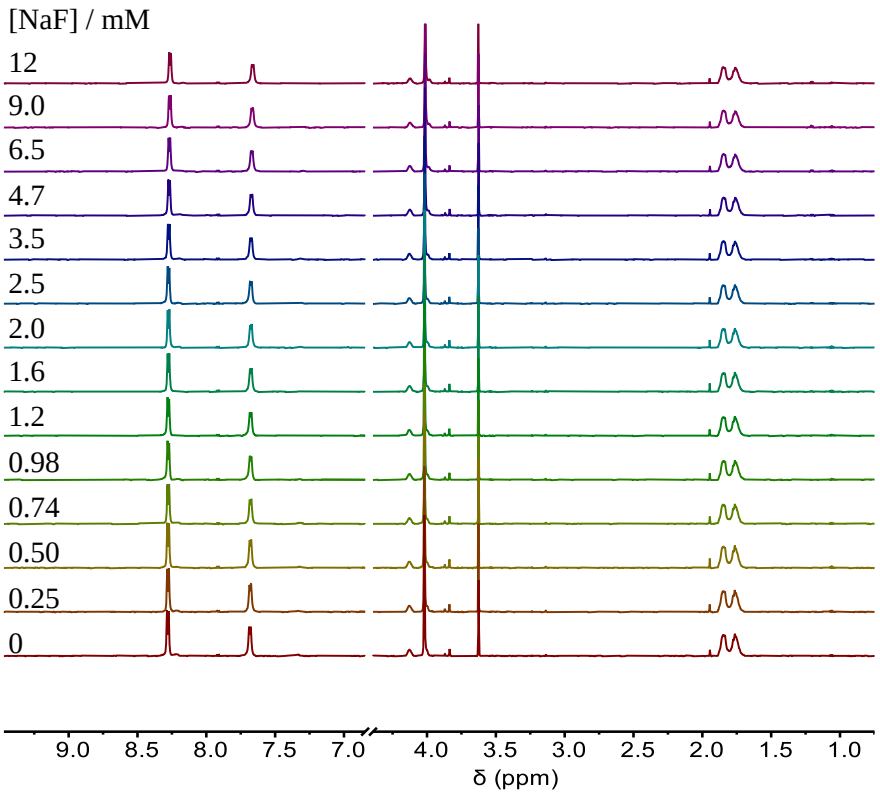

Fig. S19 ^{1}H NMR (600 MHz) titration of $\mathbf{1}^{2+}\cdot 2I^{-}$ (1 mM) with NaF in 9:1 H_2O/D_2O at 298 K. No chemical shift changes are observed.

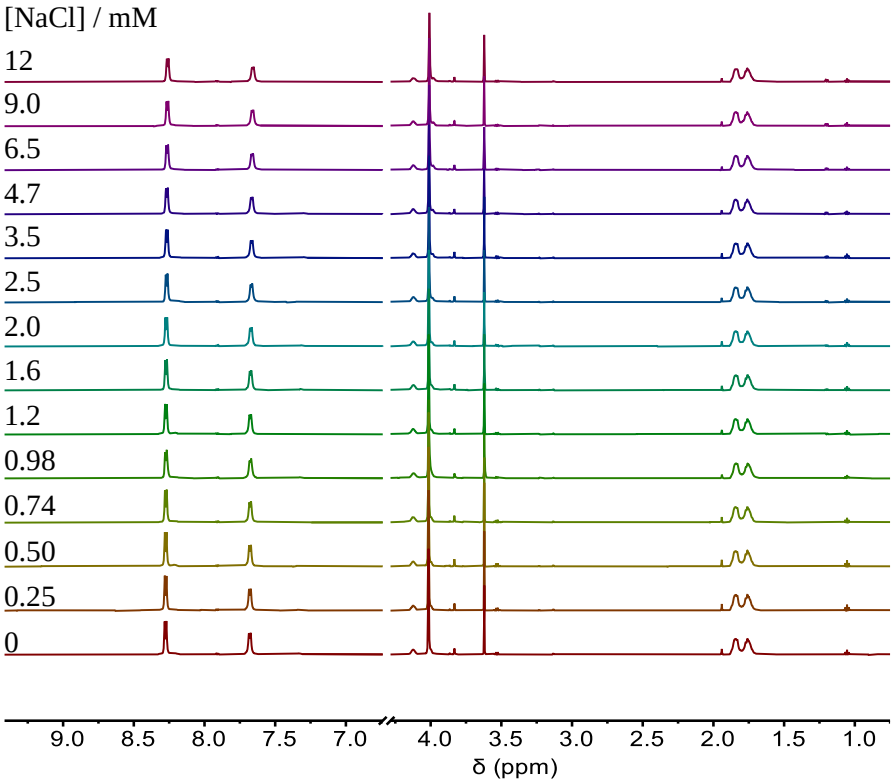

Fig. S20 ^{1}H NMR (600 MHz) titration of $\mathbf{1}^{2+}\cdot 2I^{-}$ (1 mM) with NaCl in 9:1 H_2O/D_2O at 298 K. No chemical shift changes are observed.

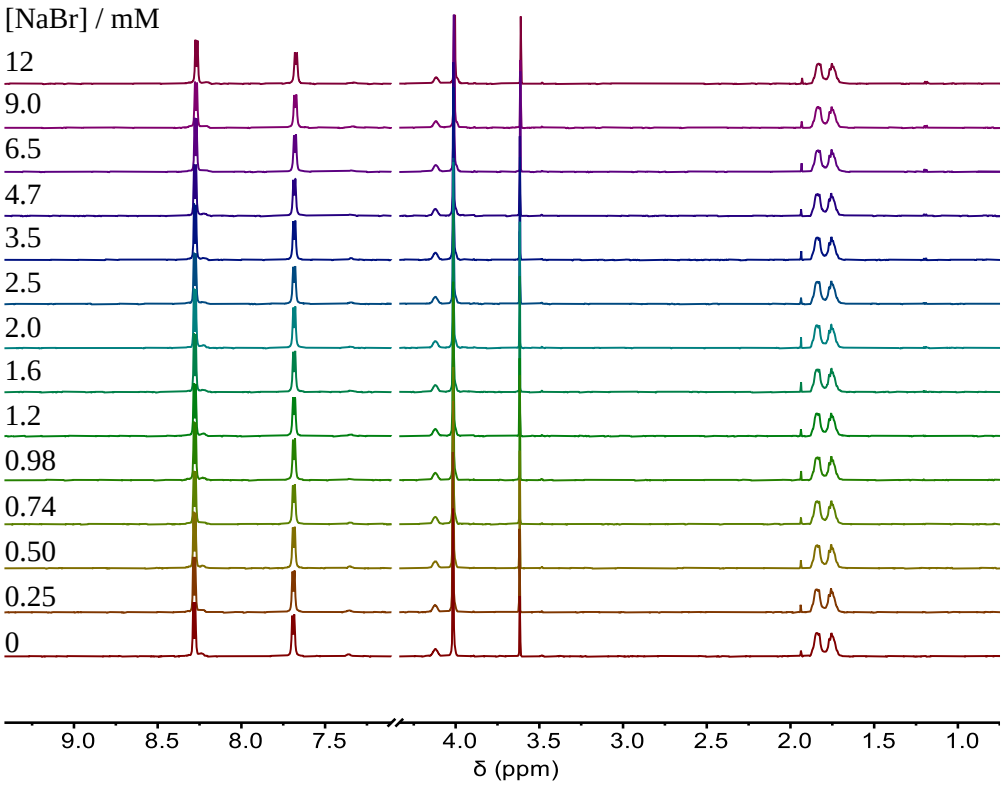

Fig. S21 ^{1}H NMR (600 MHz) titration of $\mathbf{1}^{2+}\cdot 2I^{-}$ (1 mM) with NaBr in 9:1 H_2O/D_2O at 298 K.

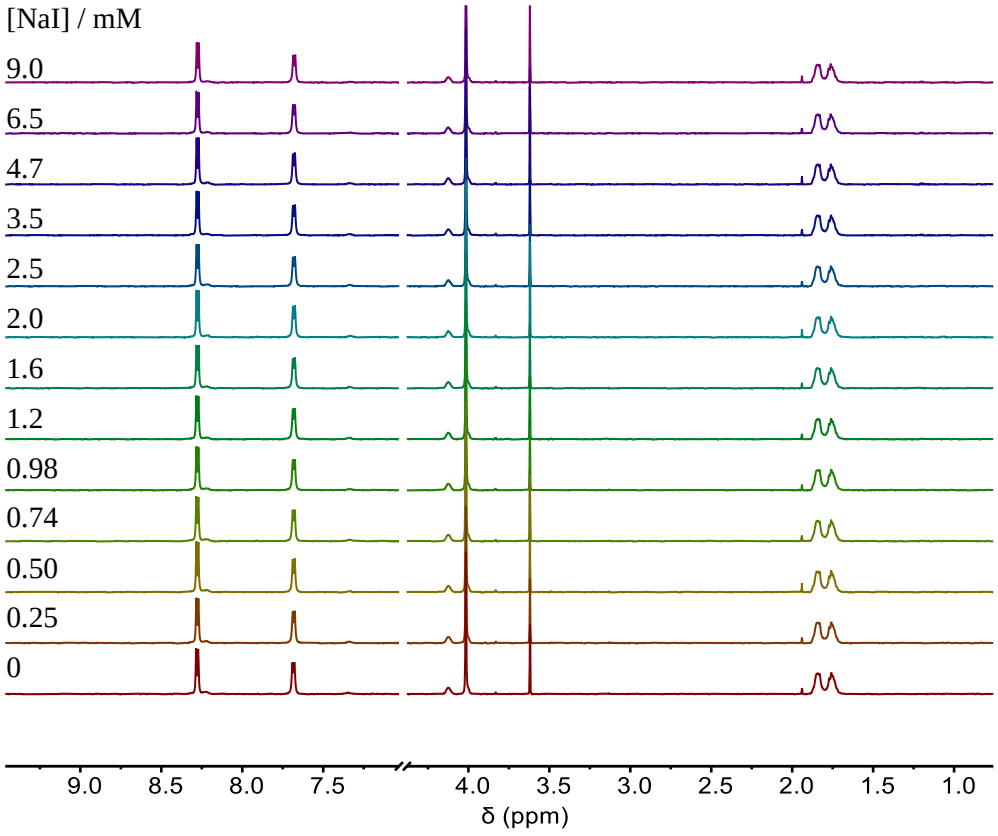

Fig. S22 ^{1}H NMR (600 MHz) titration of $\mathbf{1}^{2+}\cdot 2I^{-}$ (1 mM) with NaI in 9:1 H_2O/D_2O at 298 K. No chemical shift changes are observed.

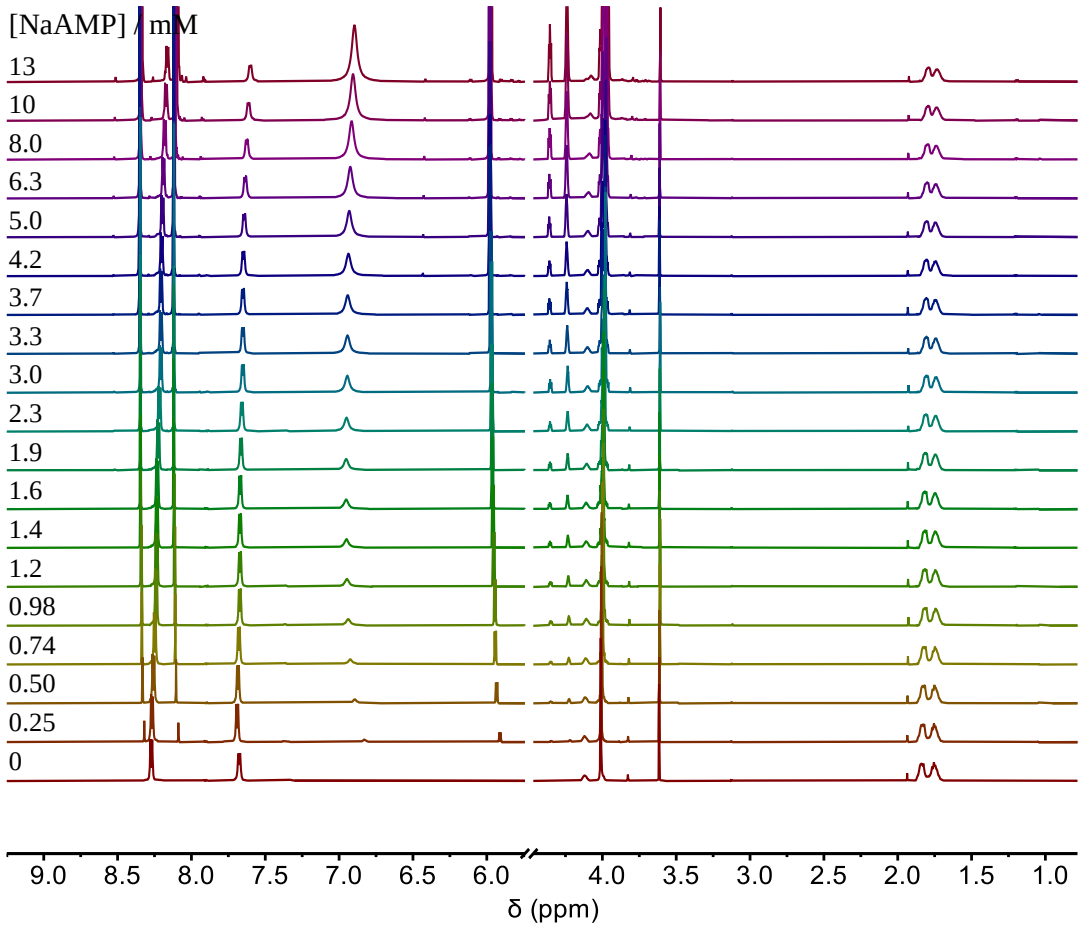

Fig. S23 ^{1}H NMR (600 MHz) titration of $\mathbf{1}^{2+}\cdot 2I^{-}$ (1 mM) with NaAMP in 9:1 H_2O/D_2O at 298 K.

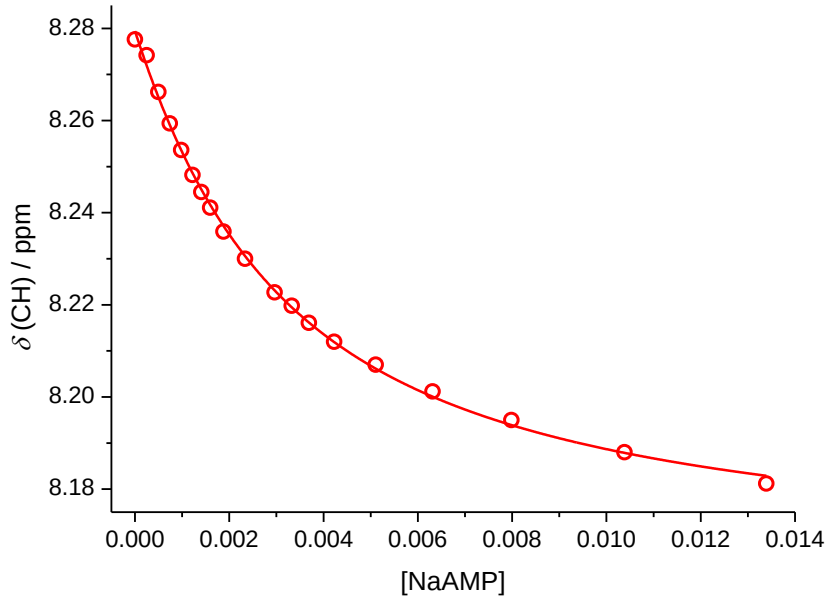

Fig. S24 Fitting of aryl CH[a] to a 1:1 binding model. *K* values of 361 and 373 M^{-1} were determined from two independent titrations, giving mean ± SD as 367 ± 8 M^{-1}.

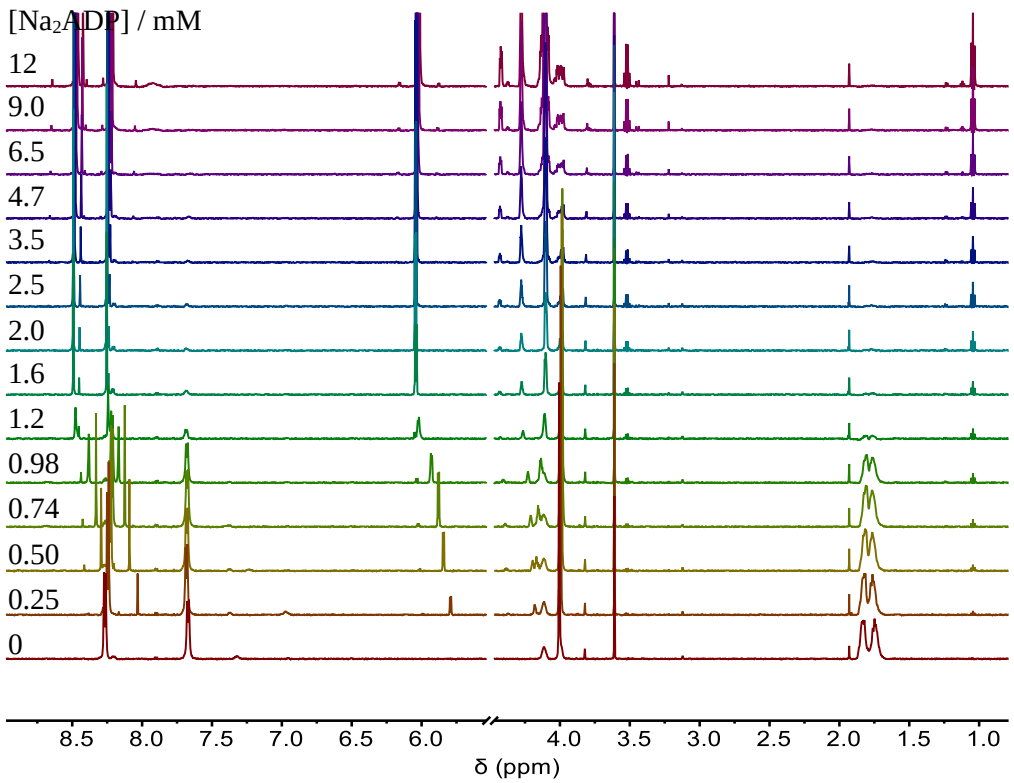

Fig. S25 ^{1}H NMR (600 MHz) titration of $\mathbf{1}^{2+}\cdot 2I^{-}$ (1 mM) with Na_2ADP in 9:1 H_2O/D_2O at 298K. Precipitation of the compounds was observed around 1 equiv. of Na_2ADP, leading to attenuation of signals from both $\mathbf{1}^{2+}$ and ADP^{2-}.

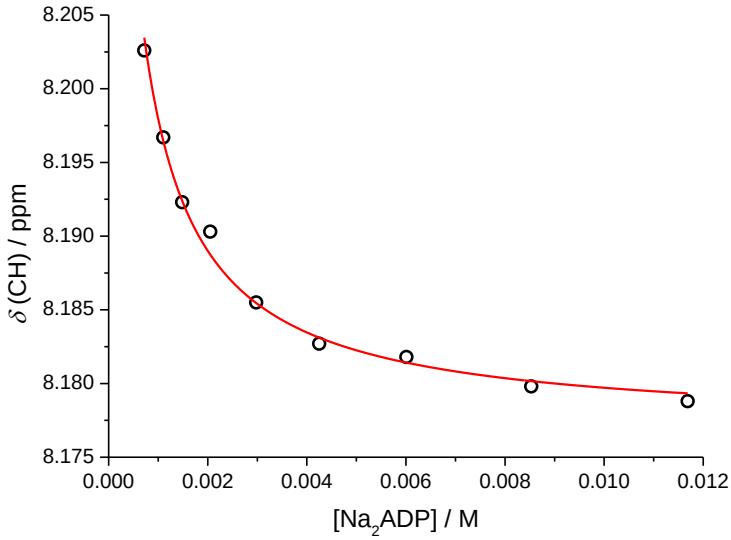

Fig. S26 Fitting of aryl CH^{a} to a 1:1 binding model, using the data points after precipitate formation was complete. Here, by performing ^{1}H NMR signal integration, we have calculated the concentrations of $\mathbf{1}^{2+}$ and ADP^{2-} that remained in the solution after precipitate formation. *K* values of 2800 and 2200 M^{-1} were determined from two independent titrations, giving mean ± SD as 2500 ± 400 M^{-1}.

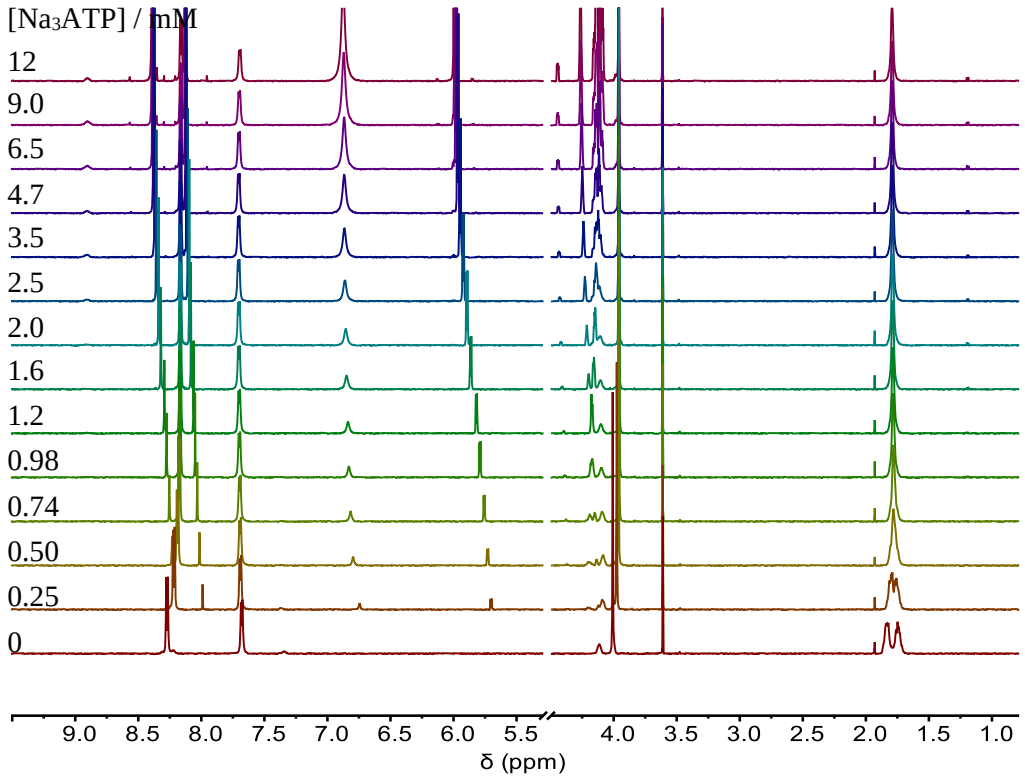

Fig. S27 ^{1}H NMR (600 MHz) titration of $\mathbf{1}^{2+}\cdot 2I^{-}$ (1 mM) with Na_3ATP in 9:1 H_2O/D_2O at 298 K.

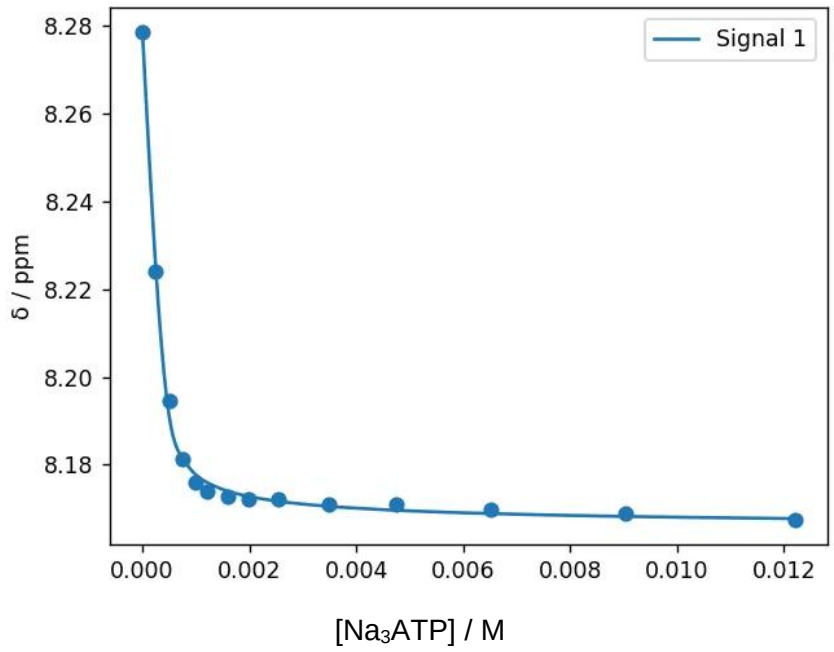

Fig. S28 Fitting of aryl CH[a] to a 2:1 binding model. β_{21} values of 6.2×10^7 and 4.0×10^7 M^{-2} were determined from two independent titrations, giving mean ± SD as $(5.1 \pm 1.5) \times 10^7$ M^{-2}.

S5. Diffusion-Ordered Spectroscopy (DOSY)

DOSY experiments were performed in 9:1 H_2O/D_2O on a 600 MHz NMR spectrometer using the stebpgp1s19 pulse sequence to suppress the water signal. The gradient strength of the NMR spectrometer was calibrated by performing a DOSY experiment of DMSO-d_6 and correcting the diffusion coefficient of DMSO-d_5 to a literature value.[3]

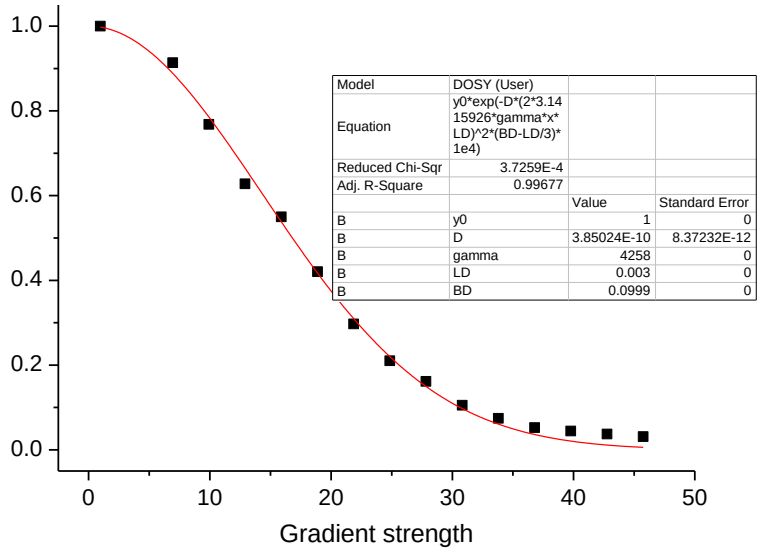

Model	DOSY (User)		
Equation	y0*exp(-D*(2*3.14 15926*gamma*x* LD)^2*(BD-LD/3)* 1e4)		
Reduced Chi-Sqr	3.7259E-4		
Adj. R-Square	0.99677		
		Value	Standard Error
B	y0	1	0
B	D	3.85024E-10	8.37232E-12
B	gamma	4258	0
B	LD	0.003	0
B	BD	0.0999	0

Fig. S29 DOSY of $\mathbf{1}^{2+}\cdot 2I^-$ (2 mM) in 9:1 H_2O/D_2O. The diffusion coefficient of $\mathbf{1}^{2+}$ is determined to be $(4.26 \pm 0.12) \times 10^{-10}$ m^{-2} s^{-1} after calibration.

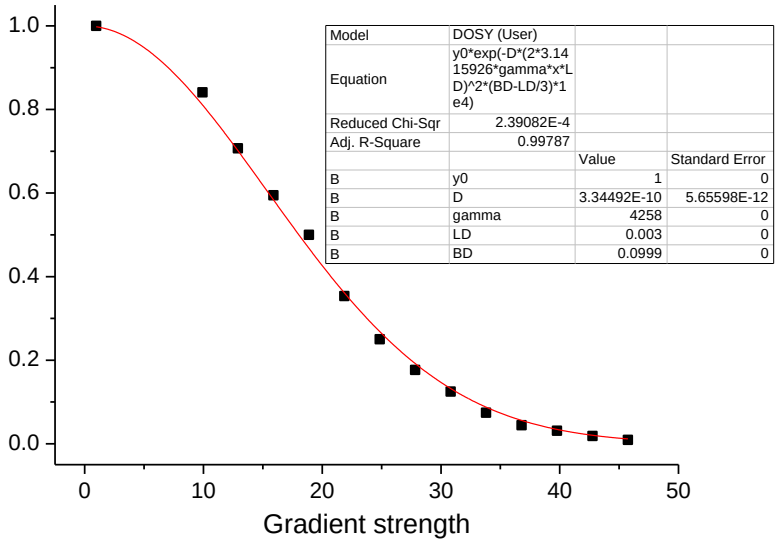

Model	DOSY (User)		
Equation	y0*exp(-D*(2*3.14 15926*gamma*x*L D)^2*(BD-LD/3)*1 e4)		
Reduced Chi-Sqr	2.39082E-4		
Adj. R-Square	0.99787		
		Value	Standard Error
B	y0	1	0
B	D	3.34492E-10	5.65598E-12
B	gamma	4258	0
B	LD	0.003	0
B	BD	0.0999	0

Fig. S30 DOSY of Na_3ATP (1 mM) in 9:1 H_2O/D_2O. The diffusion coefficient of ATP^{3-} is determined to be $(3.69 \pm 0.06) \times 10^{-10}$ m^{-2} s^{-1} after calibration.

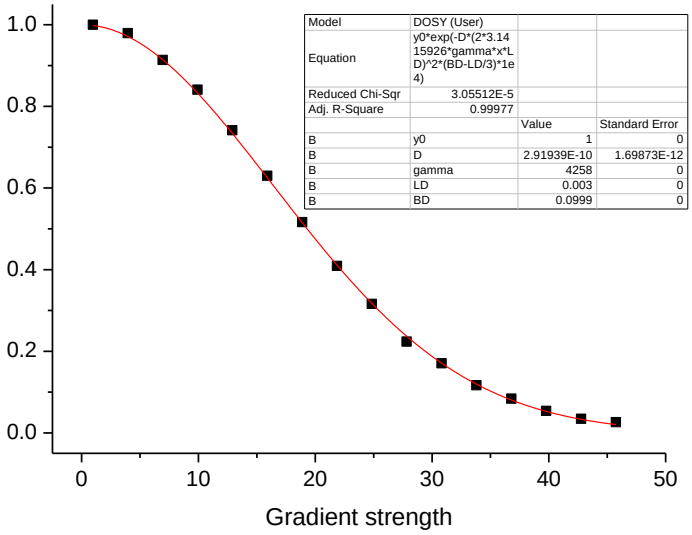

Fig. S31 DOSY of $\mathbf{1}^{2+}\cdot 2I^{-}$ (2 mM) in the presence of Na_3ATP (1 mM) in 9:1 H_2O/D_2O. The diffusion coefficient of $\mathbf{1}^{2+}$ is determined to be (3.22 ± 0.02) × 10^{-10} m^{-2} s^{-1} after calibration.

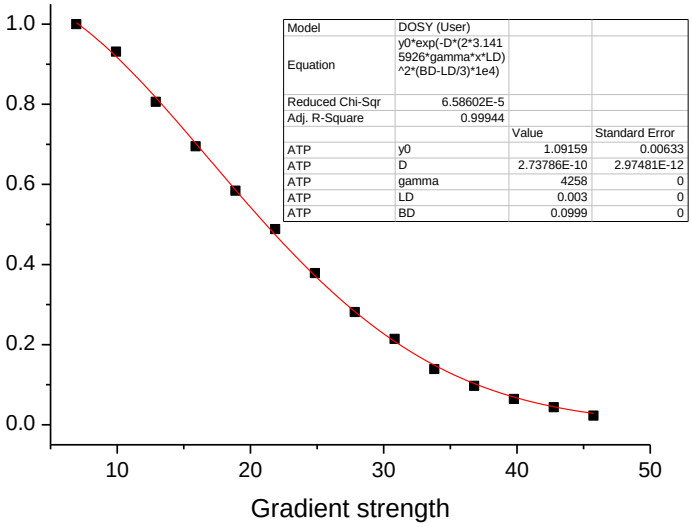

Fig. S32 DOSY of Na_3ATP (1 mM) in the presence of $\mathbf{1}^{2+}\cdot 2I^{-}$ (2 mM) in 9:1 H_2O/D_2O. The diffusion coefficient of ATP^{3-} is determined to be (3.02 ± 0.03) × 10^{-10} m^{-2} s^{-1} after calibration.

Table S1 Diffusion coefficients (*D*) of $\mathbf{1}^{2+}$ and ATP^{3-} before and after mixing

Compound	*D* / 10^{-10} m^{-2} s^{-1}	
	Before mixing	After mixing
$\mathbf{1}^{2+}$ (2 mM)	4.26 ± 0.12	3.22 ± 0.02
ATP^{3-} (1 mM)	3.69 ± 0.06	3.02 ± 0.03

S6. Computational studies

The structures of $\mathbf{1}^{2+}\cdot SO_4^{2-}$, $\mathbf{1}^{2+}\cdot HC_2O_4^-$ and $\mathbf{1}^{2+}\cdot H_2PO_4^-$ were optimized with the ωB97X-V functional[4] and def2-TZVP basis set in vacuum using Spartan'24 version 1.3.1. Input geometries were generated by placing an anion in the cavity of the neutral receptor (compound **2**) with inward pointed NH groups, followed by MMFF energy-minimization and additional of methyl groups to give $\mathbf{1}^{2+}\cdot$anion complexes.

Table S2 Cartesian coordinates for $\mathbf{1}^{2+}\cdot SO_4^{2-}$ optimized at ωB97X-V/def2-TZVP level of theory.

H	-4.679569	0.177976	-0.745072
C	-3.966543	-0.349779	-0.104125
C	-3.657678	-1.534578	2.098509
C	-2.650676	-2.560493	0.033767
C	-3.342384	-2.842704	1.367052
C	-3.422210	-1.570942	-0.858964
C	-4.608643	-0.699017	1.237467
H	-1.653446	-2.143303	0.216224
H	-4.283953	-3.382796	1.209064
H	-4.245067	-2.099068	-1.355345
H	-5.528339	-1.277540	1.087422
H	-3.140429	0.352459	0.067236
H	-4.108453	-1.739715	3.072793
H	-2.506666	-3.492725	-0.523424
H	-2.704747	-3.478581	1.989736
H	-4.884686	0.219865	1.764156
N	-2.417393	-0.790068	2.345123
H	-1.831293	-0.502100	1.549871
N	-2.509871	-1.044614	-1.878115
H	-1.979013	-0.202288	-1.600799
C	-1.945870	-1.771378	-2.819300
C	-0.788017	-1.593035	-3.575180
C	-2.245027	-3.063875	-3.515070
C	-0.974647	-2.819682	-4.355150
O	-3.078361	-3.918784	-3.406479
O	-0.406930	-3.404348	-5.250900
N	0.142423	-0.588317	-3.399244
H	-0.091605	0.098621	-2.616642
C	1.288763	-0.406852	-4.053743
N	3.688875	0.116965	-5.353347
C	1.698444	-1.176910	-5.174013
C	2.165155	0.620894	-3.596761
C	3.325107	0.846010	-4.260836

C	2.878149	-0.879970	-5.783690
H	1.090575	-2.001130	-5.538233
H	1.924972	1.169837	-2.686702
H	3.225858	-1.433852	-6.648247
C	-1.952631	-0.487943	3.536541
C	-0.794668	0.160622	3.967959
C	-2.419048	-0.670343	4.948927
C	-1.135052	0.053132	5.388959
O	-0.653784	0.375651	6.452843
O	-3.371902	-1.173586	5.475449
N	0.224540	0.632997	3.164495
H	0.111511	0.403041	2.141651
C	1.227903	1.445865	3.511224
N	3.309963	3.189206	4.111161
C	2.141657	1.874651	2.506551
C	1.435426	1.915817	4.833383
C	2.465248	2.771122	5.082020
C	3.138219	2.731151	2.840290
H	2.040502	1.551313	1.471636
H	0.792820	1.595709	5.648962
H	2.653259	3.159102	6.076517
S	0.046114	1.162607	-0.246261
O	1.484958	1.083597	-0.554606
O	-0.723934	1.034997	-1.533597
O	-0.309631	2.380549	0.461790
O	-0.328249	-0.028976	0.608901
H	3.842897	3.101722	2.104390
H	4.027803	1.610074	-3.947969
C	4.382351	4.142378	4.395375
H	5.338529	3.735807	4.060631
H	4.428418	4.317714	5.469365
H	4.188494	5.088809	3.885851
C	4.923234	0.444831	-6.066343
H	5.729985	0.600610	-5.348565
H	4.788687	1.348239	-6.666125
H	5.189576	-0.384648	-6.720445

Table S3 Cartesian coordinates for $\mathbf{1}^{2+}\cdot HC_2O_4^-$ optimized at ωB97X-V/def2-TZVP level of theory.

H	-3.933532	-0.000402	-1.142157
C	-3.314935	-0.386108	-0.325330
C	-3.382357	-1.248287	2.055936
C	-2.003935	-2.499169	0.351734
C	-2.903463	-2.621288	1.579926
C	-2.656677	-1.695491	-0.782091
C	-4.161602	-0.557683	0.936371
H	-1.065535	-2.010335	0.632635
H	-3.788669	-3.225281	1.347634
H	-3.406222	-2.320228	-1.277455
H	-5.042544	-1.173145	0.719925
H	-2.533746	0.359768	-0.150598
H	-4.022793	-1.369622	2.931291
H	-1.740958	-3.492336	-0.026879
H	-2.371053	-3.133701	2.387622
H	-4.527345	0.416386	1.275524
N	-2.242302	-0.410895	2.480630
H	-1.592317	-0.069396	1.769128
N	-1.626169	-1.382377	-1.783618
H	-0.860070	-0.797866	-1.450334
C	-1.637493	-1.845131	-3.013858
C	-0.794615	-1.768991	-4.119365
C	-2.617651	-2.691350	-3.783449
C	-1.663560	-2.576764	-4.984962
O	-3.662803	-3.214133	-3.535859
O	-1.663060	-2.983095	-6.121489
N	0.434121	-1.127997	-4.207600
H	0.765156	-0.686244	-3.350023
C	1.261529	-1.050061	-5.264536
N	3.066216	-0.831891	-7.367106
C	0.976451	-1.612886	-6.530778
C	2.496967	-0.369862	-5.110760
C	3.355135	-0.282716	-6.163205
C	1.889266	-1.481090	-7.533918
H	0.050556	-2.155220	-6.709244
H	2.764165	0.070555	-4.156164
H	1.712591	-1.897860	-8.519044
C	-1.959002	-0.204747	3.749695
C	-0.977660	0.472231	4.474454
C	-2.639253	-0.640968	5.022673
C	-1.535170	0.104674	5.784858

O	-1.272851	0.288363	6.948337
O	-3.604240	-1.293831	5.288152
N	0.135535	1.177708	4.025635
H	0.482052	0.994502	3.071833
C	0.837747	2.089887	4.722309
N	2.354486	4.008474	6.059038
C	1.952840	2.718382	4.106366
C	0.527698	2.481053	6.047708
C	1.296636	3.420641	6.665379
C	2.667186	3.652848	4.789615
H	2.231092	2.454047	3.093735
H	-0.275552	2.009238	6.602030
H	1.095380	3.736875	7.682598
H	3.521310	4.156109	4.351525
H	4.309056	0.225806	-6.086526
C	0.918205	0.540411	0.532390
C	1.814156	0.409308	-0.737494
O	1.413326	0.039001	-1.816981
O	1.539146	0.944649	1.545824
O	-0.271327	0.233409	0.408547
O	3.070402	0.743782	-0.518213
H	3.093607	0.981002	0.434622
C	3.992904	-0.678042	-8.497203
H	5.010251	-0.593951	-8.116639
H	3.739798	0.215028	-9.072163
H	3.926569	-1.557681	-9.136711
C	3.117293	5.056971	6.748553
H	4.148319	5.040888	6.396441
H	3.107335	4.860034	7.820066
H	2.675977	6.036091	6.551016

Table S4 Cartesian coordinates for $\mathbf{1}^{2+}\cdot HPO_4^-$ optimized at ωB97X-V/def2-TZVP level of theory.

H	4.681237	1.009893	0.101560
C	3.980020	0.237550	0.432391
C	3.804364	-2.128148	1.310285
C	2.389575	-0.339628	2.362982
C	3.206995	-1.603304	2.619285
C	3.196048	0.752748	1.644550
C	4.726192	-1.068971	0.708849
H	1.514354	-0.582656	1.746284
H	4.026171	-1.398310	3.318490
H	3.881184	1.221355	2.359321
H	5.542041	-0.896081	1.419294
H	3.282754	0.089818	-0.402617
H	4.357608	-3.051802	1.495152
H	2.010354	0.064184	3.307539
H	2.579535	-2.372348	3.081806
H	5.178375	-1.439124	-0.216175
N	2.728947	-2.452014	0.355699
H	2.261002	-1.686403	-0.126359
N	2.269915	1.785548	1.149199
H	1.942425	1.622336	0.203792
C	1.580957	2.574592	1.957292
C	0.418783	3.327909	1.872206
C	1.819580	3.018358	3.373438
C	0.546632	3.880779	3.234327
O	2.618816	2.751039	4.219826
O	-0.053669	4.656714	3.932279
N	-0.525502	3.354904	0.857157
H	-0.559631	2.535806	0.214336
C	-1.493243	4.269766	0.681773
N	-3.516737	6.112061	0.182491
C	-1.632126	5.437070	1.471202
C	-2.430472	4.073321	-0.367409
C	-3.406145	4.996707	-0.580261
C	-2.639858	6.311188	1.194652
H	-0.981946	5.625623	2.317709
H	-2.363892	3.186644	-0.989218
H	-2.786881	7.211389	1.780509
C	2.097012	-3.611335	0.370294
C	0.928422	-4.095070	-0.205475
C	2.381767	-4.941815	1.008785
C	1.089001	-5.452731	0.342434

O	0.498733	-6.503759	0.305722
O	3.231489	-5.373981	1.728501
N	0.011124	-3.384785	-0.966624
H	0.196384	-2.367173	-1.039958
C	-1.087791	-3.853022	-1.576947
N	-3.389763	-4.706804	-2.888222
C	-1.915080	-2.945155	-2.290477
C	-1.481666	-5.213954	-1.555385
C	-2.614656	-5.588517	-2.211226
C	-3.030879	-3.400829	-2.921212
H	-1.669633	-1.889706	-2.339140
H	-0.904812	-5.956703	-1.009568
H	-2.951260	-6.619081	-2.218057
P	0.194998	0.517151	-1.632925
O	-0.843393	1.318445	-0.928335
O	1.499200	1.447312	-1.899964
H	1.263531	2.296260	-2.293005
O	0.747579	-0.736405	-1.028491
H	-3.685121	-2.739671	-3.477580
H	-4.141477	4.885180	-1.368652
C	-4.568824	-5.173673	-3.628884
H	-5.303982	-4.370851	-3.675049
H	-5.006711	-6.023590	-3.106310
H	-4.285052	-5.471303	-4.640525
C	-4.620570	7.055612	-0.038084
H	-5.488514	6.765560	0.557730
H	-4.884554	7.057273	-1.095214
H	-4.298712	8.056706	0.246897
O	-0.381050	0.207391	-3.106673
H	0.260494	-0.275485	-3.642018

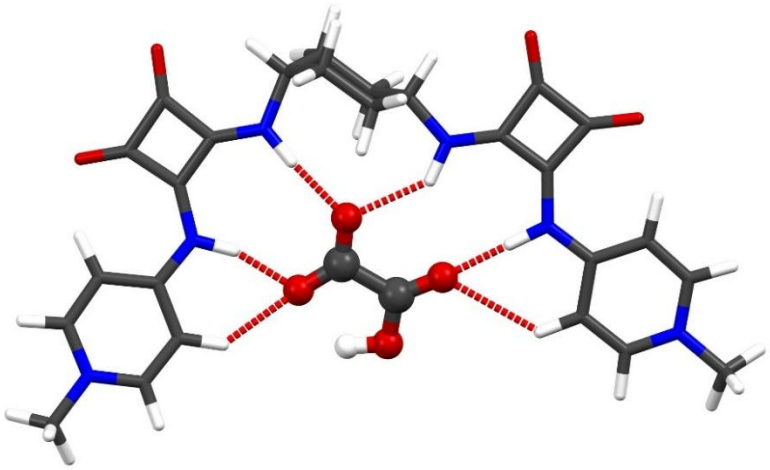

Fig. S33 $\mathbf{1}^{2+}\cdot HC_2O_4^-$ complex optimized at ωB97XV/DEF2-TZVP level of theory.

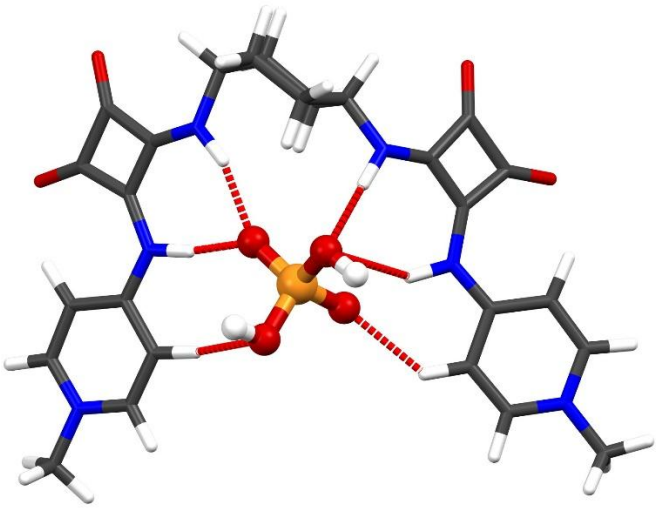

Fig. S34 $\mathbf{1}^{2+}\cdot H_2PO_4^-$ complex optimized at ωB97XV/DEF2-TZVP level of theory.

S7. References

1. M. K. Christensen, K. D. Erichsen, U. H. Olesen, J. Tjørnelund, P. Fristrup, A. Thougaard, S. J. Nielsen, M. Sehested, P. B. Jensen, E. Loza, I. Kalvinsh, A. Garten, W. Kiess and F. Björkling, *J. Med. Chem.*, 2013, **56**, 9071-9088.
2. D. O. Soloviev and C. A. Hunter, *Chem. Sci.*, 2024, **15**, 15299-15310.
3. R. Evans, Z. Deng, A. K. Rogerson, A. S. McLachlan, J. J. Richards, M. Nilsson and G. A. Morris, *Angew. Chem. Int. Ed.*, 2013, **52**, 3199-3202.
4. N. Mardirossian and M. Head-Gordon, *Phys. Chem. Chem. Phys.*, 2014, **16**, 9904-9924.